Geomechanics and Engineering, *Vol. 28, No. 6 (2022) 585-598*
https://doi.org/10.12989/gae.2022.28.6.585

Simulation of monopile-wheel hybrid foundations under eccentric lateral load in sand-over-clay

Xinjun Zou[1a], Yikang Wang[1b], Mi Zhou[*2] and Xihong Zhang[3c]

[1]*College of Civil Engineering, Key Laboratory of Building Safety and Energy Efficiency of Ministry of Education, Hunan University, Changsha, Hunan 410082, China*
[2]*School of Marine Science and Engineering, State key laboratory of subtropical building science, South China University of Technology, 381 Wushan Rd, Guangzhou, Guangdong 510640, China*
[3]*School of Civil and Mechanical Engineering, Curtin University, Kent Street, Bentley 6102, Australia*

(Received January 9, 2021, Revised February 10, 2022, Accepted February 12, 2022)

Abstract. The monopile-friction wheel hybrid foundation is an innovative solution for offshore structures which are mainly subjected to large lateral eccentric load induced by winds, waves, and currents during their service life. This paper presents an extensive numerical analysis to investigate the lateral load and moment bearing performances of hybrid foundation, considering various potential influencing factors in sand-overlaying-clay soil deposits, with the complex lateral loads being simplified into a resultant lateral load acting at a certain height above the mudline. Finite element models are generated and validated against experimental data where very good agreements are obtained. The failure mechanisms of hybrid foundations under lateral loading are illustrated to demonstrate the effect of the friction wheel in the hybrid system. Parametric study shows that the load bearing performances of the hybrid foundation is significantly dependent of wheel diameter, pile embedment depth, internal friction angle of sand, loading eccentricity (distance from the load application point to the ground level), and the thickness of upper sandy layer. Simplified empirical formulae is proposed based on the numerical results to predict the corresponding lateral load and moment bearing capacities of the hybrid foundation for design application.

Keywords: failure mechanism; FEM; lateral load and moment bearing capacities; monopile-friction wheel hybrid foundation; offshore wind turbine

1. Introduction

1.1 Conception

Offshore wind turbines (OWT) are developing overwhelmingly in recent years which are extending to deeper water for acquiring higher power density (Li *et al*. 2016). The monopile foundation is one of the most widely used substructure types for OWTs because of its economic and relatively mature technology features (Fatahi *et al*. 2020, Chong *et al*. 2019). Increasing the pile diameter and embedment length are found to be effective but may not be feasible in more severe environments because of its higher costs and installation difficulties (Chen *et al*. 2020). Hence, there is a practical demand for optimization of traditional monopile foundations to meet the demands of new generation OWTs.

The hybrid monopile-friction wheel foundation is a combination of traditional monopile foundation and circular friction footing (see Fig. 1), which is initiated from designs of pile caps and embedded retaining walls with stabilizing platforms (Xu *et al*. 2020). The addition of wheel provides large shear stress for enhancing the lateral bearing capacity, because of which the length of the monopile can be reduced. The friction wheel also provides scour protection which ameliorates the long-term performance of the OWT. Therefore, the hybrid foundation provides a broader adaptability for more severe offshore conditions. It has the potential to greatly improve the performance of foundation system for OWT, while minimizing the installation cost and time (Wang *et al*. 2018a). However, the performance of this type of hybrid foundation particularly in complex soil condition is still not fully understood. The feasibility of hybrid foundations is also challenged for its constructability, such as transportation and accurately positioning the friction wheel to the designed offshore location. Driving the pile into the friction wheel with a restricted tolerance in underwater environment is also a challenge. Sand-underlaying-clay soil deposit is one of the most commonly encountered soil conditions in some petroleum and renewable energy active regions, e.g. in the Yellow Sea of Korea, North Sea, Gulf of Mexico, South China Sea, offshore India and Thailand (Zou *et al*. 2018). Many researchers have reported the load bearing behaviors of different types of foundations in this sand-overlaying-clay soil profiles (Zou *et al*. 2018, Hossain *et al*. 2019,

∗Corresponding author, Associate Professor
E-mail: zhoumi@scut.edu.cn
[a]Professor
E-mail: xjzouhd@hnu.edu.cn
[b]Research Fellow
E-mail: wangyk@hnu.edu.cn
[c]Senior Research Fellow
E-mail: xihong.zhang@curtin.edu.au

ISSN: 2005-307X (Print), 2092-6219 (Online)

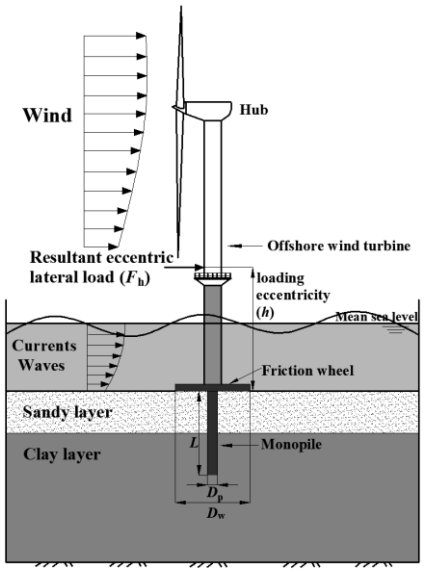

Fig. 1 Schematic diagram of offshore wind turbine foundation system on monopile-friction wheel hybrid foundation

Bandyopadhyay *et al*. 2020). Meyerhof and his co-workers (Meyerhof and Hanna 1978) found that "punching-through" failure would occur in the two-layer soil, where the sand block would penetrate the underlaying clay when vertical compression from the upper footing occurs. Hence, previous understandings in pure sand or clay soil conditions may not be applicable in depicting the bearing performance of hybrid foundations in sand-over-clay soil deposit. A systematic study is still badly needed.

1.2 Previous work

Previous studies mainly investigated the lateral load and moment bearing performances of monopile-friction wheel hybrid foundations in pure sand or clay soil deposits, which focused on the following four issues: (1) load transfer mechanisms of introducing friction wheel; (2) the behavior of hybrid monopile foundations under combined static loading; (3) the influence of foundation geometry on the bearing capacity; (4) the load bearing performance of hybrid foundations in cyclic and seismic loading conditions. In terms of the load transfer mechanism of hybrid foundations, previous studies were conducted including 1g model tests, centrifuge tests, simplified analytical derivations and finite element modellings (Lehane *et al*. 2014, Yang *et al*. 2018, EI-Marassi 2011). It was found that the restoring moment provided by the friction wheel plays a dominant role in the load and moment bearing capacities of the hybrid system. In addition, the lateral load and moment were initially undertaken by the wheel component, while the pile came to effect as the pile lateral displacement increased. Both laboratory test and numerical modeling have been carried out to study the combined load bearing performance of the hybrid foundation (Arshi *et al*. 2016, Wang *et al*. 2018a, Trojnar 2019). The lateral stiffness and load bearing capacity were found to be apparently improved by adding the friction wheel in sand and clay soil under cyclic and seismic loading conditions. Trojnar (2019) carried out a series of full-scale field tests on monopile-friction wheel hybrid foundation in dense and loose sands. It was found that the hybrid foundation had a better performance than the monopile with smaller lateral deflections. Considering the complex offshore site condition, the constructability is also crucial in the design (Liu *et al*. 2020). For newly installed hybrid foundations, it is suggested that the seabed should be levelled first to ensure the full-contact between the friction wheel and mudline. Then the wheel should be towed to the designed site and used as a targeting location for the installation of the pile. There are two ways of connecting the pile and friction wheel, i.e. coupled and decoupled approaches, which can be referred to the research of Stone *et al*. (2018).

There is still very limited study on the bearing performance of hybrid foundations in sand-over-laying-clay soil deposit (Zou *et al*. 2018). To provide better understanding, in this study the failure mechanisms and loading characteristics of hybrid foundations in sand-overlaying-clay soil are examined numerically. A numerical model is generated using ABAQUS which is validated with a small-scale model test. Extensive parametric study is then carried out to estimate the detailed behaviors of the hybrid foundation and the pile–soil interaction in sand-over-laying-clay deposit where the influences of different design parameters are evaluated. Empirical design formulae are proposed based on numerical results for quick estimation of the lateral load and moment bearing capacities of the hybrid foundation for engineering application.

2. Methodology

2.1 Numerical modeling and boundary conditions

Small strain finite element analyses are employed for all the investigations by using the commercial software ABAQUS (Dassault Systèmes 2016). Fig. 2 illustrates the three-dimensional semi-cylindrical model of the monopile-friction wheel foundation in sand-overlaying-clay soil deposits. The installation process is not simulated in this study. A hybrid foundation for 3.6 MW capacity OWT with typical pile diameter D_p = 4 m and wall thickness t_p = 40 mm the size of transition part connected on the friction wheel as 4 m in height with a 5 m outer diameter. Three geometrical variables are considered, i.e., the wheel diameter D_w, pile embedment length L and wheel thickness T_w, as listed in Table 1. Relatively fine mesh size is adopted near the foundation/soil interface, and coarser mesh is employed for the rest region to reduce the computation time. The soil domain extends sufficiently far away from the foundation to avoid the influence of boundary effect ($2D_w$ distance from wheel edge to width boundary (H_{BD}) and $1L$ distance from pile end to height boundary (V_{BD}), as shown in Fig. 2). Considering symmetry, only half of the foundation with soil is modeled, and the bottom of the soil is fully fixed.

2.2 Material model and parameters

The monopile and friction wheel are modelled using elastic material model with steel properties i.e., Young's

modulus E_p = 210 GPa, density of 7850 kg/m^3 and Poisson's ratio υ = 0.17. The pile and wheel are coupled together to simulate rigid grouting connection. The tower is modelled using rigid elements with null unit weight, and the pre-vertical load is applied to the reference point of the tower head to simulate the dead weight of the wind turbine structure (Chen *et al*. 2020, Anastasopoulos and Theofilou 2016), as shown in Fig. 2. The sand is modelled as an elastic-perfect-plastic material with Mohr-Coulomb yield criterion and non-associated flow law. The foundation structure/soil interaction has commonly modelled with the classical Mohr-Coulomb model by different researchers in previous numerical analyses (Gourvenec and Barnett 2011, Feng *et al*. 2014). Mohr-Coulomb model was found to be able to well capture the soil behavior and yielded reasonable prediction of the bearing capacity of foundations under static loading conditions (Raj *et al*. 2019). Three-dimensional 8-nodes (3 degrees of freedom per node) linear brick elements are used for the soil. To quantify the influence of the top sandy soil, the material properties for the top sand are varied in the numerical simulation, where friction angle j varies from 23° to 40° and dilation angle ψ = φ - 30° (ψ is taken as 0 when φ is less than 30° (Li *et al*. 2013)). The other material properties are kept as constants which are referred to commonly used silica sand in centrifuge tests (Wang *et al*. 2018b) and a series of laboratory tests, including the Young's modulus of sand E_s (40 MPa), cohesion c (0 kPa), Poisson's ratio, υ (0.3) and effective unit weight γ'_s (9.8 kN/m^3). The underlying clay is assumed to vary linearly with submerged soil depth as

$$s_u = s_{um} + kz \tag{1}$$

where s_{um} is the undrained shear strength at mudline, which increases linearly with a gradient k as the submerged depth z below the soil surface develops. The Young's modulus E_c of clay is set as 500s_u varying linearly with soil depth which follows previous studies (Zhou *et al*. 2016). The effective unit weight γ'_c is 8.5 kN/m^3 and the Poisson's ratio is 0.49 to model the fully undrained condition. All the values are for kaolin clay with material constants used in centrifuge tests (Yang *et al*. 2018). To study the influence of sand layer thickness on the lateral load and moment bearing capacities of the hybrid foundation, it is varied with the ratio of T_s/L from 0.1 to 1. It is assumed that there is no tension at the interface between the pile and the sandy soil behind the loading direction following experimental observation, while that in front of the pile foundation at pile end is also ignored because of negligible tensile response in lab tests. Interactions between pile and sand, and wheel and sand are simulated by using perfect contact with Coulomb's tangent friction model. Detachment and sliding are allowed during the loading process. A thin layer of interface elements is employed to the pile and clay interface with the shear strength penalty of αs_u, where α is the interface friction coefficient. This method can consider the interaction between the foundation and soil, which is commonly adopted in small strain finite element analyses by other researchers (Gourvenec and Barnett 2011, Gourvenec and Mana 2011). The penalty factors α for the interfaces of

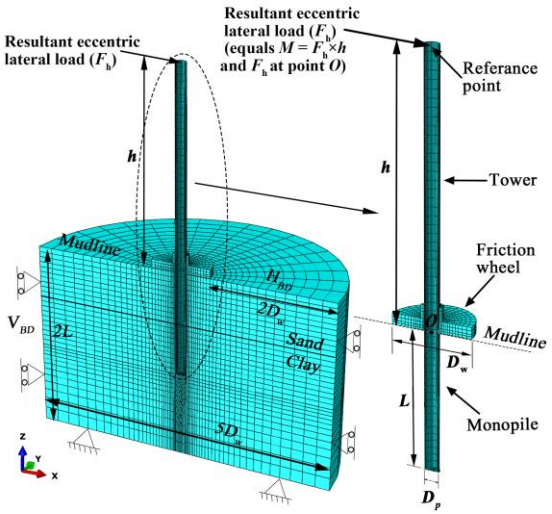

Fig. 2 Geometry and mesh of hybrid foundation models

sand/pile and clay/pile are both set as 0.4 following empirical data derived from laboratory results (Yang *et al*. 2017). The resultant lateral load (F_h) at a particular loading height (h) above the seabed is arising from action of water wave, current and wind force acting on the turbine tower, which equals to the lateral load (F_h) and moment (M = $F_h \times h$) acting at the mudline. The reference point (RP) is located at the surface coupling center of tower head for applying lateral and pre-vertical load with displacement-controlled probes as shown in Fig. 2 (Yang *et al*. 2017). The bearing capacity is often defined as the turning point of the load-displacement curves. However, in some cases, it is difficult to identify such a point by the above criterion. Therefore, a more commonly used criterion of the rotation angle θ = 5° is used to define the ultimate capacity (DNV 2019, Li *et al*. 2020). It is worth noting that despite in reality the loads applied to the foundation is dynamic which could influence the real behaviour of the foundation system, the dynamical effect is usually simplified and considered with a dynamic amplification factor in design to predict the bearing capacity of the foundation structure (Gourvenec and Barnett 2011, API 2014, DNV 2019).

3. Model validation

To verify the above numerical model, a small-scale model test was carried out to explore the failure mechanism and load bearing behavior of the hybrid foundation in sand-overlaying-clay as shown in Fig. 3(a) (Group I, Table 1). The homogeneous clay soil sample used is obtained by mixing the de-aired water and the undisturbed soil which is obtained from South China sea through a mixer in a steel vessel. The liquid and plastic limits of this clay are 47.7% and 26.6%, respectively. And the average undrained shear strength, inferred from shear vane tests, is 3.3 kPa at the surface of the clay profile after preparation. The sand used is Fujian standard sand with a mean particle diameter D_{50} of 0.35 mm, void ratio limits of 0.61 to 0.95. The relative density of the fine dry sand is controlled as 65% by

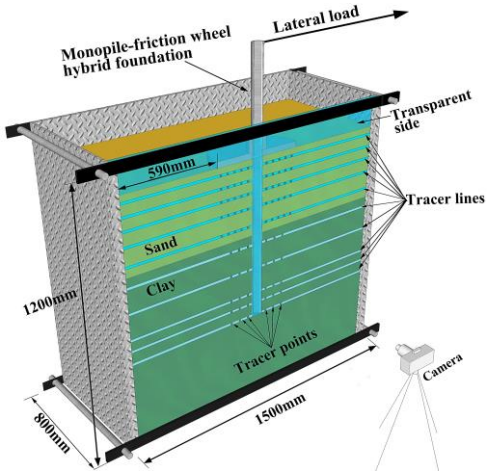

(a) Test setup and dimensions

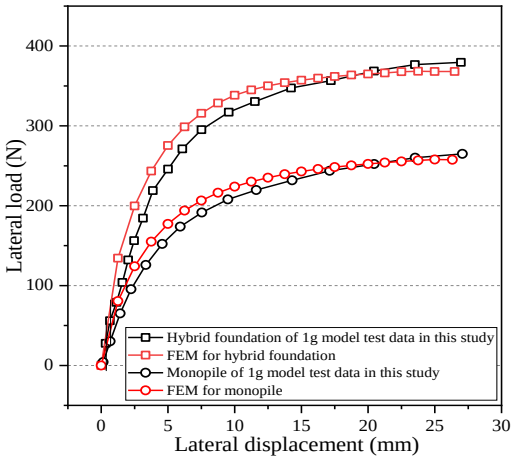

(b) Q-S curves comparison

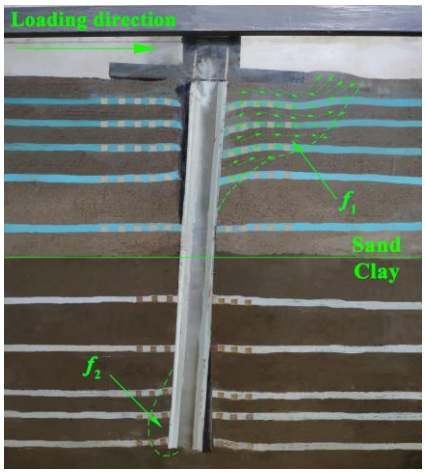

(c) Small scale model test

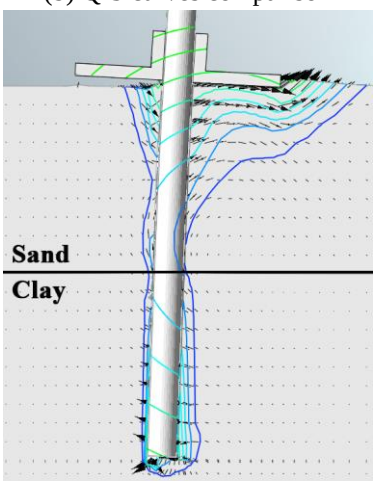

(d) FE result

Fig. 3 Validation of numerical study against small scale model test

adopting air pluviation method during filling. The soil is confined within an in-house-designed strongbox with internal size of 1500 mm (length) × 800 mm (width) × 1200 mm (depth) and with a transparent glass window to allow observation of the soil deformations around the foundation in sand-overlaying clay deposits. The soil sample is divided into twelve layers by setting tracer lines including five layers for lower clay layer and seven layers for the upper sandy layer. The soil movement can be captured by the camera through the tracer lines of colored silica sand and tracer points of red dots positioned near the side of glass during the test. To prevent soil from entering the gap between the hybrid foundation and window, two thin layers of non-sticky foams are attached along the two opposite edges of the pile. The model pile is fabricated with a hollow semi-circular aluminum pipe with 48-mm-outer diameter (D_p), 2-mm-wall thickness (t), 620-mm-embedded length and the friction wheel is a 320-mm-diameter and 20-mm-thickness aluminum disc. It yields a scale ratio of 1:42 for the corresponding prototype pile with a diameter of 2 m, wall thickness of 0.08 m and pile length of 25 m, combined with a friction wheel of 13 m for the wheel diameter and 0.96 m in thickness. The pile and wheel were fixed together through a threaded hole on the side of a flanged collar which was connected to the friction wheel. Pre-installation method is adopted for the pile by fixing the model pile in the predetermined position after filling the clay to the bottom of pile toe. The surrounding soil is backfilled until reaching the design thickness of soil layer. Then, the friction wheel is placed at the mudline and connected to the pile through the flanged collar. The lateral load is imposed on the pile head by means of pulley and weight blocks attached to a flexible wire rope and the laser displacement transducer is installed at the height of loading position for the measurement of lateral displacement. In the present tests, every loading step is sustained for a period of time, and the next load step is executed only when the lateral deflection is relatively stable to ensure measurement accuracy.

In terms of lateral load-displacement reactions, the overall observation suggests that the numerical model reliably reproduces the lateral load and moment bearing behaviors of the monopile and hybrid foundation in sand-overlaying clay deposits in Fig. 3(b). Soil deformation around the hybrid foundation is depicted in Figs. 3(c) and 3(d). It can be seen that soil flow mechanism between the model test and FE simulation agrees very well. According to the soil movement characteristics when approaching the

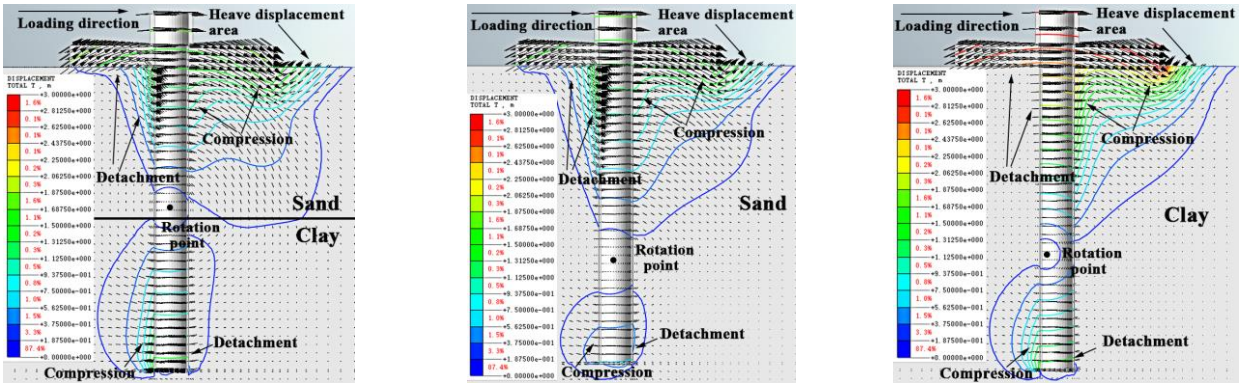

(a) Sand-overlaying-clay (b) Pure sand (c) Pure clay

Fig. 4 Displacement nephogram in ultimate condition

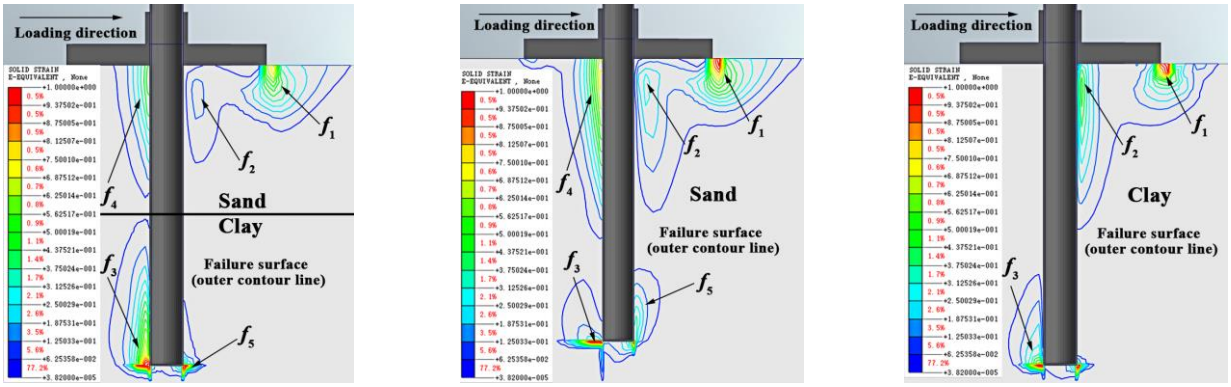

(a) Sand-overlaying-clay (b) Pure sand (c) Pure clay

Fig. 5 Range of equivalent plastic strain in ultimate condition

ultimate condition, the wedge-shape deformation area (f_1) near the mudline in front of the loading direction propagates down along the right side of the pile to a depth of about 80% thickness of the sandy layer. It extends in the loading direction to the range of about 75% of the wheel radius away from the right wheel edge at the mudline. This is because the hybrid foundation experiences the lateral translation to the right along with clockwise rotation and the soil is compressed and motivated due to the friction resistance and passive earth pressure near the pile side and under the wheel. Significant subsidence of the wheel and heave displacement of the sandy soil are captured near the mudline in front of the loading direction. Because of the sliding and rotational translation of the foundation, the sandy soil located in the rear side of the hybrid foundation experiences tension as the foundation disengages from the soil mass, causing a depression on the mudline and further settlement of the sand soil along the left body side of the pile. In addition, the soil compression (f_2) occurs near the pile end on the left-hand side and detachment is captured at the right side of the pile end as the rotational translation develops.

4. Failure mechanisms under lateral load

To better understand the behavior and failure mechanism of hybrid foundations in sand-overlaying-clay soil under lateral eccentric load, the soil displacement vectors and plastic strain contours in the ultimate bearing condition are summarized and plotted in Figs. 4 and 5. The soil displacement vectors and failure mechanism of the monopile-friction wheel hybrid foundation in sand-overlaying-clay is shown in Figs. 4(a) and 5(a) with typical material properties and dimensions, i.e. D_w = 24 m, T_s/L = 0.5, φ = 31°, s_{um} = 30 kPa, k = 1 kPa/m (Group II, Table 1). Another two cases are also plotted for comparison including: (i) hybrid foundation in sand only (D_w = 24 m, φ = 31°, Group III) as in Figs. 4(b) and 5(b); (ii) hybrid foundation in clay (D_w = 24 m, s_{um} = 30 kPa, k = 1 kPa/m, Group VI) as in Figs. 4(c) and 5(c). The other parameters for all the three cases are D_p = 4 m, L = 36 m, h = 60 m, α = 0.4, e_w = 0 m, T_w = 2.5 m.

From Fig. 4(a), it can be observed that the rotation center of the foundation is captured near the interface of the two layers with slightly upwards movement. With the increase of lateral eccentric load, compression in the sandy soil is found on the right part of the foundation which leads to a large area of heave displacement near the wheel edge and a downward displacing sector shape beneath the wheel. In addition, noticeable compression occurs on the left side facing of pile near its end. In the opposite elevation of the pile in lower clay layer, detachment occurs along the pile, and sand detaching can also be captured under the wheel facing the loading direction. As can be seen in Figs. 4(b)

and 4(c), when the hybrid foundation is in pure sand or pure clay, the rotation center position of the hybrid foundation moves to lower locations along the pile, and less soils are disturbed near the pile end on both sides. It is also worth noting that the deformation of soils appears to be smaller on the right side of the wheel in pure clay in Fig. 4(c) as compared to that in pure sandy soil and sand-overlaying-clay conditions. In addition, at the right side of pile under the wheel, the downwards soil deformation indicates that the presence of clay layer underlaying the sand layer has a large influence on the lateral load bearing performance of the hybrid foundation through comparison with those in Figs. 4(a) and 4(b). In terms of the plastic strain contour as depicted in Figs. 5(a)-5(c), several plastic strain zones are observed when the hybrid foundation is in sand-overlaying-clay, pure sand, and pure clay soil deposits. As for the effect of the friction wheel, a hill-type failure surface is developed under the wheel at right-hand side near the exterior edge (f_1). Because of the rotation of the pile, the compressive forces lead to the plastic deformation area along the pile underneath the wheel (f_2), as well as the far ends of the pile near its end (f_3). Corresponding to the detachment area discussed above, an elongated semi-raindrop shape zones can be captured under the wheel on the left part of pile (f_4) along with a minor detachment area on the right part of pile near its end (f_5) in Figs. 5(a) and 5(b). When the hybrid foundation is in pure sand, the area of f_1 is evidenced to be widen in the horizontal direction compared to Fig. 5(a). As for the hybrid foundation in pure clay soil condition, the areas of f_1 and f_3 shrink evidently, while f_2 is seen to be enlarged. Similar displacement and plastic strain distribution for hybrid foundations in pure sand soil deposit were also reported by other researchers (El-Marassi 2011, Arshi *et al*. 2016).

5. Parametric study

5.1 Influence of wheel diameter (D_w/L)

Previous study indicates that the lateral load and moment bearing capacities of hybrid foundations could be highly related to the ratio of wheel diameter over the pile length (Yang *et al*. 2018). To quantify the influence of wheel diameter on the lateral load bearing performance of the hybrid foundation, a group of numerical models with wheel diameter D_w = 0, 6 m, 10 m, 16 m, 18 m, 20 m, 22 m, 24 m and 26 m with pile embedment depth L = 30 m, 36 m and 40 m are simulated (D_w/L = 0~0.72, φ = 31°, h/D_p = 15, V = 5 MN, T_s/L = 0.5, T_w/D_p = 0.63, e_w = 0 m, s_{um} = 30 kPa, k = 1 kPa/m, Group V, Table 1). The normalized lateral load bearing capacity versus normalized wheel diameter curves are plotted and shown in Fig. 6(a). It can be seen that the lateral load and moment bearing capacities increase with the increase of D_w. A noteworthy trend is captured that the increasing rate per D_w/L raises quickly beyond a critical value of 0.4 for L = 30 m and 0.5 for L = 40 m, and the relationship keeps almost linearly afterwards. Substantial plastic deformation is developed near the inner side under the wheel edge, which appear to be nonuniform. Relatively larger plastic deformation area can be captured near the pile body and the right edge of wheel as D_w/L increases. With D_w/L exceeding 0.5, the expansion of plastic strain zone becomes more distinct in the corresponding area, which results in additional passive pressure and resorting moment as the pile rotates. Similar phenomenon can also be identified for hybrid foundations (Stone *et al*. 2018) in pure sand soil deposit from centrifuge test. Fig. 6(b) depicts the passive earth pressure along the pile body when the hybrid foundation reaches the ultimate state. The lateral contact soil pressure is normalized as $P_p/(2\pi R^3\gamma')$, where the effective unit weight γ' is taken as γ'_s in the upper sandy layer and γ'_c in the lower clay layer, respectively. Obvious differences can be captured between the hybrid foundation and monopile in the lateral earth pressure on the rear side of the loading direction. It is worth noticing that D_w/L influences the lateral earth pressure of the hybrid foundation in three aspects: 1) the value of the maximum lateral earth pressure increases, and the position rises on the right-hand side with the increase of D_w/L; 2) the rotation center (depth at $P_p/(2\pi R^3\gamma')$ = 0) of the foundation moves upwards which manifests better stability against overturning with the increase of D_w/L; 3) the lateral earth pressure increases significantly near the ground surface on the right-hand side when D_w/L increases. This is because as the soil bearing area underneath the wheel increases, the vertical stresses in front of the pile increases, which leads to soil densification under the wheel. As shown in the lateral soil stress cloud diagram of the hybrid foundation and monopile presented in Fig. 6(b), it is similar to the results of centrifuge tests on hybrid foundations in sand (Wang *et al*. 2018a). It can be observed that the lateral earth pressure adjacent to the sand/clay interface increases significantly as z/L elevates compared to that of the hybrid foundation in pure sand as reported by Trojnar (2019). This is because that the soil stress redistributed at the interface of two layers of soil with different deformability, which results in the influence on the lateral and moment bearing behaviors of the hybrid foundation. However, the difference of the lateral earth pressure distribution is sufficiently small to be ignored when D_w/L is beyond 0.44, which means the vertical stress resulted from the wheel contributes no further enhancement to the lateral soil resistance along the pile. Fig. 6(c) shows the vertical passive earth pressure distribution under the wheel. The distribution of the vertical bearing pressure increases with the distance d_w/D_p away from the pile center. And it experiences a sudden reduction when approaching the wheel edge. As can be seen in the vertical soil stress distribution diagram in Fig. 6(c), the maximum stress zone locates under the wheel in the range of $0.5R_w$-$0.8R_w$ (R_w is the radius of the wheel) in this case. The results from previous studies by Lehane *et al*. (2014) are provided for comparison (as shown in Fig. 6(c)). In general, the total vertical soil resistance improves with the increase of D_w/L because of the increased bearing area. Thus, it can be concluded that increasing the wheel diameter (D_w/L) has an evident enhancement effect on the horizontal resistance of the hybrid foundation.

5.2 Influence of pile length (L/D_p)

To study the influence of pile length on the lateral load and moment bearing capacities of hybrid foundations, numerical modeling is conducted by varying the pile length from 30 m to 42 m (L/D_p = 7.5 to 10.5), keeping other parameters constant (D_w/L = 0.67, h/D_p = 15, V = 5 MN,

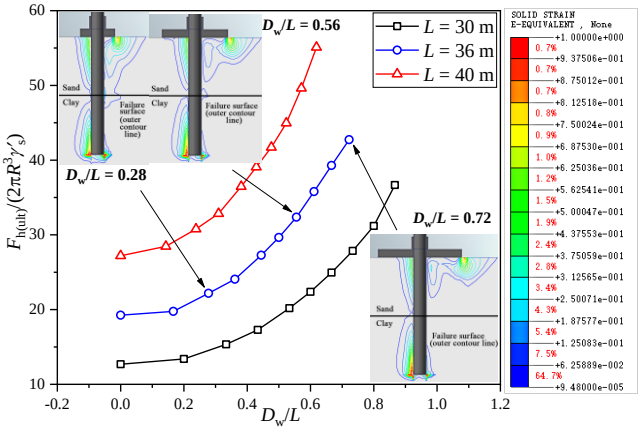

(a) The trend of lateral bearing capacity and failure mechanism with different wheel diameters

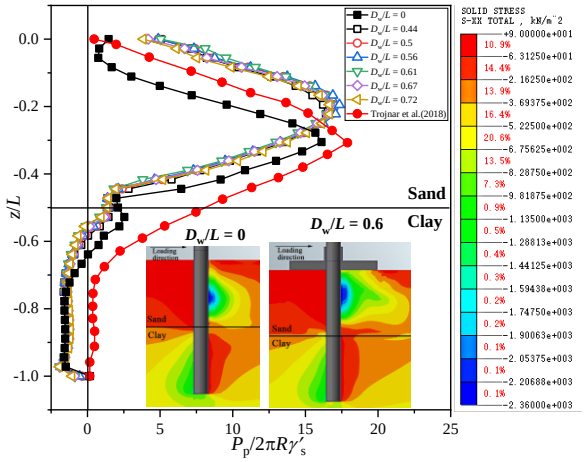

(b) Lateral contact earth pressure along pile

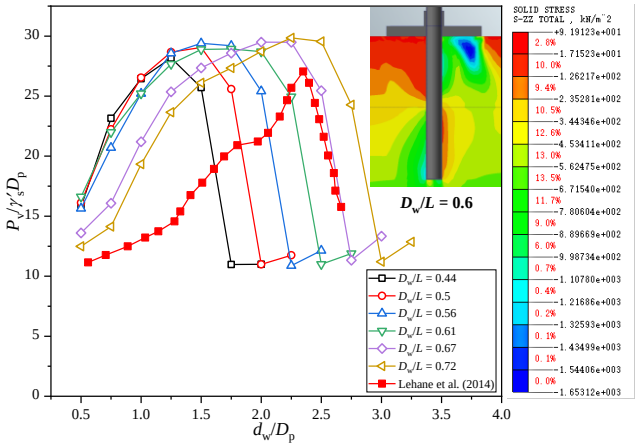

(c) Vertical passive pressure under wheel

Fig. 6 Influence of wheel diameter on lateral capacity performance

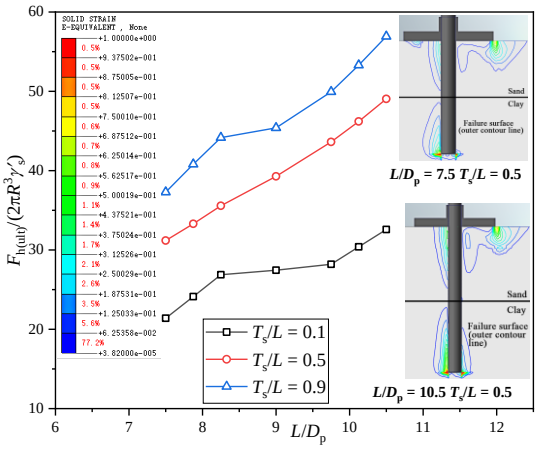

(a) The trend of lateral bearing capacity with different pile lengths

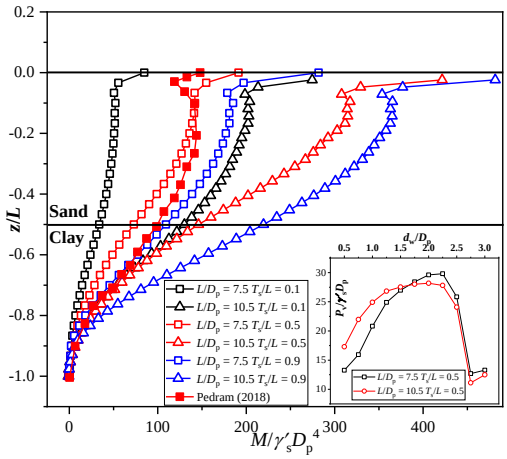

(b) Bending moments along pile with different pile embedment lengths

Fig. 7 Influence of pile embedment length on lateral bearing capacity and failure mechanisms

T_s/L = 0.1, 0.5 and 0.9, T_w/D_p = 0.63, e_w = 0 m, s_{um} = 30 kPa and k = 1 kPa/m, Group VI, Table 1). The relation between the lateral load and moment bearing capacities and the pile embedment length is shown in Fig. 7. It can be seen in Fig. 7(a) that as pile length increases, an obvious positive effect on the load bearing capacity is achieved. In addition, the curve shows three typical regions: when T_s/L = 0.1 and 0.9, while it keeps in almost linear manner as for T_s/L = 0.5. For example, the slope of the curve drops when L/D_p = 8.25 for both T_s/L = 0.1 and 0.9, and it sharply increases at L/D_p = 9 and 10 when T_s/L = 0.1 and 0.9, respectively. In addition, when T_s/L increases from 0.1 to 0.9, an overall increasing

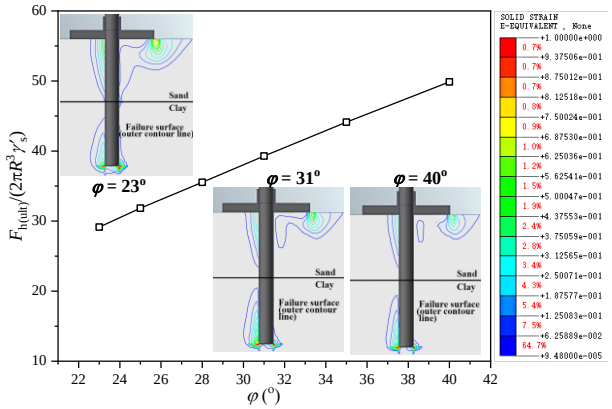

Fig. 8 Influence of internal friction angle of sand

trend can be found on the load bearing capacity for the foundation with different L/D_p. This is because a longer pile provides more contact area to resist the lateral load which can be found in the plastic strain contour as depicted in Fig. 7(a). And the thickness of the sandy layer has an obvious influence on the relationship of capacity and pile embedment length. Fig. 7(b) demonstrates the bending moment distribution along the pile with different pile embedment depths and sandy layer thicknesses. The maximum bending moment locates at depth of about $0.15L$ and a turning point of the moment locates at $z/L = 0.5$. Fig. 7(b) compares the numerical results with that by Pedram (2018) in pure sand (L = 15 m, D_p = 5 m, D_w = 16 m, h/D_p = 12, φ = 30°, T_s/L = 1, e_w = 0 m). As L/D_p increases from 7.5 to 10.5, the overall bending moment along pile increases significantly, especially for the maximum moment and the moment near the ground surface. And a larger T_s/L is also beneficial for the increase of the bending moment when T_s/L increases from 0.1 to 0.9. This is because that the enhancement of the lateral bearing resistance for greater pile embedment depth is mainly provided by the soil resistance along the pile body which results in the increase of pile deflection and moment. And the vertical earth pressure under the wheel barely changes as L/D_p increases, as shown in Fig. 7(b). It can be concluded that the load bearing capacity increase for hybrid foundations with greater pile length.

5.3 Influence of internal friction angle of sand (φ)

To examine the influence of internal friction angle φ, a group of analyses are carried out with different φ, while D_w/L = 0.67, h/D_p = 15, V = 5 MN, T_s/L = 0.5, T_w/D_p = 0.63, e_w = 0 m, s_{um} = 30 kPa and k = 1 kPa/m, Group VII, as shown Table 1. Normalized $F_{h(ult)}/2\pi R^3\gamma'_s$-$\varphi$ curve is plotted in Fig. 8, in which it is obvious that the hybrid foundation exhibits better lateral load bearing performance with the increase of φ, almost showing a positive proportional relationship between $F_{h(ult)}$ and φ. The plastic strain zone is evidently reduced around the foundation as φ increases from 23° to 40°. This is because the increase of internal friction angle leads to a larger soil stiffness, which therefore results in a higher soil resistance and then leads to higher lateral load and moment bearing capacities. The similar conclusion was reported by Yang *et al*. (2017) for bucket foundation in sand, in which the stable platform bearing behavior was found to be similar for both the bucket and hybrid foundations. It can be concluded that the lateral load and moment bearing capacities of the hybrid foundation are closely related and positively proportional to the internal friction angle of sand.

5.4 Influence of loading eccentricity (h/D_p)

The distance from loading point to soil surface (loading eccentricity) leads to different bending moments applied to the hybrid foundation. To examine the influence of loading eccentricity, a group of numerical models are generated with varying ratios of loading eccentricity h/D_p = 11.25, 15, 18.75, 22.5, 26.25 and 30, while the other parameters are kept the same as D_w/L = 0.67, φ = 31°, V = 5 MN, T_s/L = 0.5, T_w/D_p = 0.63, e_w = 0 m, s_{um} = 30 kPa and k = 1 kPa/m, Group VIII, as shown in Table 1. As shown in Fig. 9(a), the load bearing capacity of the foundation decreases as h/D_p increases. The plastic strain diagrams are used to depict the lateral bearing behavior at the ultimate state. It can be observed that relatively larger plastic failure zones are developed under the right-hand side of wheel and near the left-hand side of the pile end when h/D_p = 30 in comparison to that of h/D_p = 11.25. This is because the bending moment induced by the load eccentricity accelerates the soil around the foundation to develop into the plastic stage which speeds up the hybrid foundation to approach the limiting state. The failure of the hybrid foundation is dominated by the lateral movement and more soil around the pile needs to be mobilized with lower ratio of h/D_p. Hence the hybrid foundation exhibits a higher load bearing capacity. As the loading height increases, the failure is progressively dominated by rotational translation which exert the restoring moment provided by the wheel. It accelerates the soil plastic zone development in the area beneath the wheel as the wheel rotates, which diminishes the load bearing capacity. Similar findings were reported by Li *et al*. (2014) for modified suction caissons in sandy soil, where the horizontal load and moment bearing capacities were found to increase by 83% when the ratio of h/D_p decreased by 50%. Fig. 9(b) compares the distributions of the bending moment along the pile under different loading heights. It can be seen that the location of the maximum bending moment moves upwards slightly, and the value of the maximum bending moment increases evidently, whose tendency decelerates as the load eccentricity increases.

When z/L is near the mudline, the bending moment experiences an extinct reduction at about z/L = -0.05, then it undergoes a sudden increase at the mudline along with a sharp decline within the height of friction wheel as z/L moves upwards. Fig. 9(b) also shows that the vertical passive pressure raises as the loading height elevates, which indicates that the main contribution of the friction wheel to the lateral and moment bearing capacities is by providing additional restoring moment. Similar phenomenon was reported in Pedram's research from numerical results of hybrid foundation in pure sand (Pedram 2018).

5.5 Influence of sand layer thickness (T_s/L)

To quantify the influence of the top sand layer thickness on the lateral load bearing capacity of the hybrid foundation, a group of simulations with varied normalized

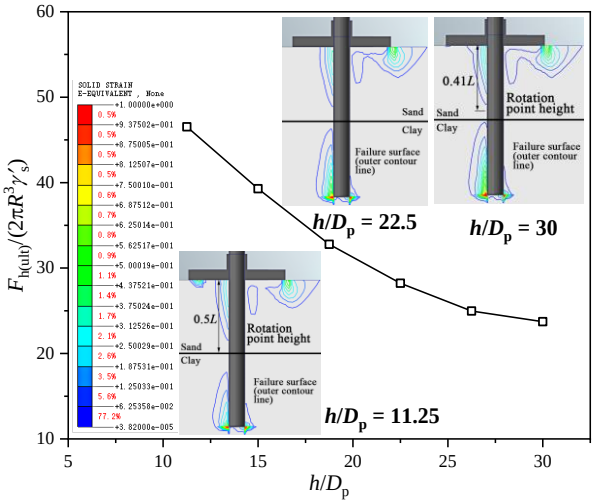

(a) The effect of loading eccentricities

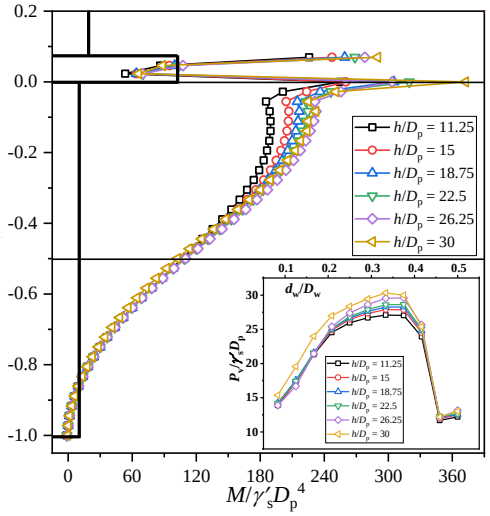

(b) Bending moments along the pile

Fig. 9 Influence of loading eccentricity on lateral capacity

thickness ratios of sandy layer are conducted (T_s/L = 0.1, 0.2, 0.3, 0.4, 0.5, 0.7, 0.8, 0.9 and 1), while the other parameters are kept constant (D_w/L = 0.67, φ = 31°, h/D_p = 15, V = 5 MN, T_w/D_p = 0.63, e_w = 0 m, s_{um} = 30 kPa and k = 1 kPa/m, Group IX, as shown in Table 1). Fig. 10 describes the relationship between the normalized load bearing capacity and sand layer thickness. The lateral load and moment bearing capacities increase almost linearly as T_s/L increases within the range of 0.1~0.3, and the slope of the curve decreases when T_s/L = 0.3~0.7. As T_s/L is beyond 0.7, the trend begins to accelerate and maintains a nearly linearly increase. The variation range of equivalent plastic strain on the right-hand side under the wheel of T_s/L = 0.9 is found to be larger than that when T_s/L = 0.5. As for the failure mechanism of the hybrid foundation in T_s/L = 0.1, an obvious "punching–through" failure can be captured on the right-hand side underneath the wheel. The mechanism contains a rigid block right beneath the wheel, a passive wedge at the right-hand side of the wheel in the sandy layer, and a fan within the clay layer. Similar conclusion was drawn from the failure mechanism reported by Zheng *et al.* (2018) of the strip footing under combined load in sand-over-clay soil condition.

Fig. 11 demonstrates the velocity diagrams for various values of T_s/L. For a sand layer with T_s/L = 0.1, a large amount of soil deformation area develops in the clay layer. The failure surface penetrates the soft clay, which leads to a reduced bearing capacity, indicating the possibility of punching shear failure. With an increase in T_s/L from 0.1 to 0.3, the failure surface in the clay layer is greatly reduced, as shown in Figs. 11(a) and 11(b), which demonstrates the improved bearing capacity results from increasing the depth of the sand layer. When T_s/L exceeds a certain "critical depth", the failure surface is completely confined within the sand layer. The minimum depth is denoted as the critical sand thickness at which the failure surface develops completely within the sand layer (in this case T_s/L is slightly less than 0.5). As can be seen in Fig. 11, the failure zone shrinks as the thickness of sandy layer increases from T_s/L =

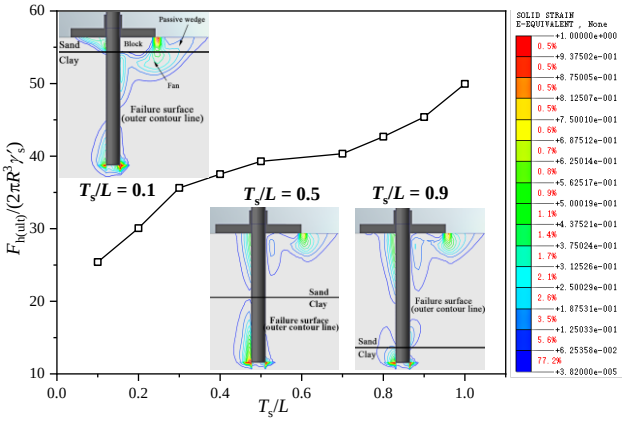

Fig. 10 The effect of sandy layer thicknesses

0.1 to 0.5 at the right margin of the wheel in front of the loading direction. In addition, the increase of sandy layer thickness results in upward movement of the rotation center and the trend decelerates. Based on these observations, it can be reasonably concluded that a thicker sand layer helps to improves the lateral load and moment bearing capacities and the lateral stability of the hybrid foundation.

5.6 Influence of pre-vertical load (V) and thickness of wheel (T_w/D_p)

The initial bearing pressure under the wheel from the gravity of the super structures is a nonnegligible influencing factor that should be taken into consideration for the hybrid foundation system (Trojnar 2019). In engineering practice, superstructure loads range between 2 MN to 10 MN for wind turbines of 3 MW to 7.5 MW (Malhotra 2011). In this study, ten cases of pe-vertical loading conditions are analyzed (V = 2 MN, 4 MN, 6 MN, 8 MN and 10 MN, acting on the pile and the plate respectively), among which five cases are applied at the reference point of the pile head and another five are applied on the wheel upper surface

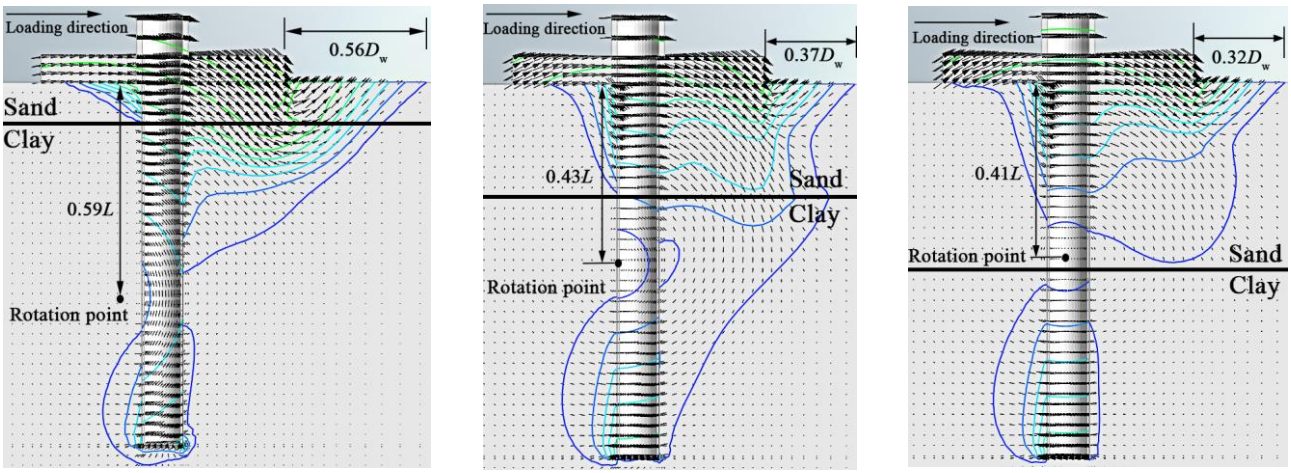

(a) T_s/L = 0.1 (b) T_s/L = 0.3 (c) T_s/L = 0.5

Fig. 11 Soil flow mechanism with different sandy layer thicknesses

with vertical distributed pressure. (D_w/L = 0.67, φ = 31°, h/D_p = 15, T_s/L = 0.5, T_w = 2.5 m, e_w = 0 m, s_{um} = 30 kPa and k = 1 kPa/m, Group X, Table 1). Fig. 12 shows the normalized lateral load-displacement curve under different pre-vertical loading conditions. It can be concluded that with the increase of pre-compression, the lateral load bearing capacity improves slightly both in two arrangements of the hybrid foundation. The difference of the failure mechanisms of V = 2 MN and 10 MN is sufficiently small to be ignored in the present configuration. This is because that almost all the vertical load is undertaken by the wheel in both arrangements of the hybrid foundation in sand-overlaying-clay soil deposits, and the pre-vertical load in practical engineering results slight vertical settlement of the foundation and barely changes the initial pressure beneath the wheel. Similar conclusion was also reported by Yang *et al*. (2018) in their centrifuge tests on hybrid foundations in sand.

The initial contact at the wheel/soil interface is also relevant to the thickness of wheel, which provides pre-vertical load from its self-weight. In addition, the passive pressure acting on the wheel subsidence part has a potential influence on the load bearing capacity which cannot be neglected in practice. In order to investigate the pre-vertical load effect of the solid steel wheel and the influence of the wheel subsidence on the lateral bearing behavior of the hybrid system, four cases of analyses are conducted with T_w = 1 m, 2.5 m, 4.5 m and 6.5 m, and another three cases with the pre-vertical load as a constant for reference by applying vertical distributed vertical pressure on the wheel surface of T_w = 1 m with q = 117 kPa (equals to T_w = 2.5 m), q = 273 kPa (equals to T_w = 4.5 m) and q = 429 kPa (equals to T_w = 6.5 m). (D_w/L = 0.67, φ = 31°, V = 5 MN, h/D_p = 15, T_s/L = 0.5, e_w = 0 m, s_{um} = 30 kPa and k = 1 kPa/m, Group XI, Table 1). Fig. 13 depicts the normalized lateral load - displacement curves with different thicknesses of wheel and equivalent vertical distributed pressures. The lateral bearing behavior improves as the thickness of wheel increases in a nearly linearly manner, as shown in Fig. 13. From the plastic strain distributions of T_w/D_p = 1.625 and q = 429 kPa, the failure mechanism of increasing the thickness of

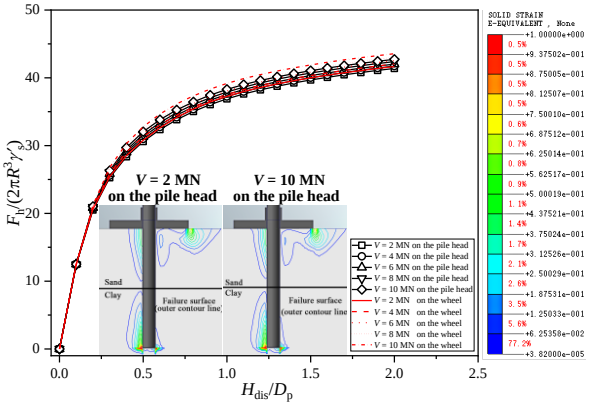

Fig. 12 Lateral load-displacement curves with different pre-vertical loadings

wheel is similar to that of increasing the pre-compression. In addition, the enhancement of the capacity by increasing the thickness of wheel is slightly higher than that by increasing the equivalent distribute pressure. It can be concluded that a thicker wheel improves the lateral bearing behavior mainly through the pre-vertical load from its self-weight. However, the transportation and installation of such a large and heavy friction wheel can be costly and difficult to implement based on the literature and current engineering practice (Chen *et al*. 2020, Anastasopoulos and Theofilou 2016). Hence, gravel wheel and lightweight circular footing with backfilled rubble were proposed for cost saving and increasing pre-vertical load (Yang *et al*. 2018, Anastasopoulos and Theofilou 2016). In conclusion, the thickness of the friction wheel has a certain influence on the lateral and moment bearing capacities but should not be considered as one of the major controlling factors during design compared to the other influencing factors.

5.7 Influence of undrained shear strength of the lower clay (kD_p/s_{um})

To study the influence of undrained shear strength of the lower clay, Fig. 14 shows the results for normalized

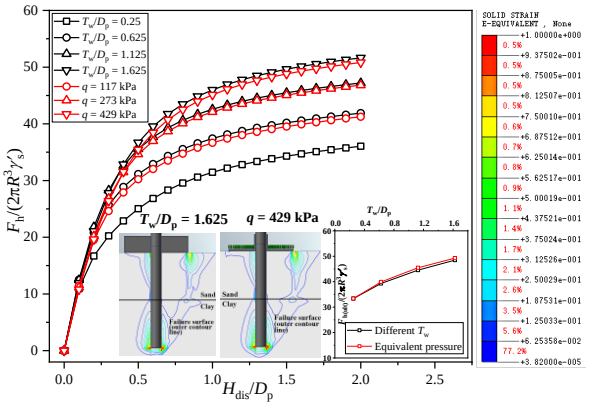

Fig. 13 Lateral load-displacement curves with different thicknesses of friction wheel

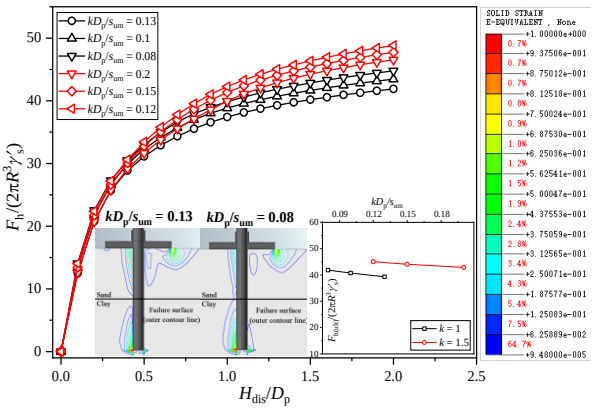

Fig. 14 Lateral load-displacement curves with undrained shear strength of lower clay

horizontal load–displacement curves with varying s_{um} = 20 kPa, 30 kPa, 40 kPa, and 50 kPa with k = 1 and 1.5 (kD_p/s_{um} = 0.08, 0.1, 0.12, 0.13, 0.15, 0.2) (Group XII, Table 1). It is apparent that undrained shear strength of clay has a slight influence on the lateral load bearing capacity of the hybrid foundation. With the increase of gradient k, the lateral load bearing capacity experiences a limited improvement. This confirms that the difference caused by undrained shear strength of clay layer is not substantial and can be neglected for design purposes.

6. Empirical design formulae

From the above parametric study, it is confirmed that wheel diameter (D_w), pile embedment depth (L), loading eccentricity (h), and thickness of upper sandy layer (T_s) have evident influences on the lateral load bearing capacity of the hybrid foundation. Although the wheel thickness surely has a nonnegligible effect on the lateral bearing performance, it is unrealistic and uneconomical for the manufacturing and transportation of the friction wheel with a large thickness. Therefore, the average thickness of the wheel is kept constant as 2.5 m which is considered representative and reasonable for practical OWT structures (Anastasopoulos and Theofilou 2016). An average internal friction angle of sand 33° is adopted for saturated fine sand

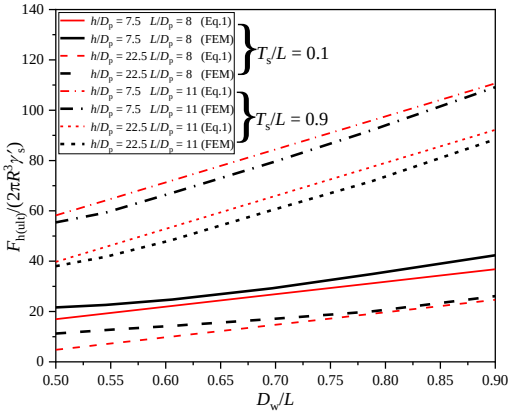

Fig. 15 Comparison between results from FEM and the prediction of the empirical formula

in most cases (Zou *et al*. 2018, Lehane *et al*. 2014, Yang *et al*. 2018). Empirical formula is derived for predicting the lateral load bearing capacity of hybrid foundation systems. Since the superstructure loads range between 2.6 MN to 7 MN for 3 MW to 5 MW wind turbines (Malhotra 2011), a typical dead weight of 5 MN is adopted during the analyses. The hybrid foundation is made of steel material with properties of E_p = 210 GPa, υ = 0.17 and density of 7850 kg/m^3. All the values of the influencing factors are based on the existing project status in formulas. According to the discussion about the effect of T_s/L, the values of T_s/L are divided into ranges of T_s/L are divided into ranges of $0.1 < T_s/L \le 0.3$, $0.3 < T_s/L \le 0.7$, and $0.7 < T_s/L \le 1$. Formulae of initial fitting can be obtained by selecting the appropriate iteration. The normalized lateral load and moment bearing capacities are utilized to fit the curve, which represent all the data points adequately. Empirical expressions are derived to determine the lateral bearing capacity for preliminary design of a hybrid foundation. Table 2 lists values of the coefficients related to T_s/L and L/D_p.

$$\frac{F_{h(ult)}}{2\pi R^3\gamma'_s} = a + b\times\left(\frac{D_w}{L}\right) - c\times\left(\frac{h}{D_p}\right) \quad (2)$$

Fig. 15 compares the difference between the prediction of Eq. (2) and the FEM results (h/D_p = 7.5 & 22.5; L/D_p = 8 and 11; T_s/L = 0.1 and 0.9; D_w/L = 0.5~0.9). As can be seen in Fig. 15, the results calculated by Eq. (2) agree well with that predicted by FEM, which means that the empirical formula is suitable to predict the bearing capacity of the hybrid foundation in this study.

In order to verify the suitability of the above empirical formulae, the load bearing capacity of the hybrid foundation from Eq. (2) is compared with the centrifuge tests result reported by Lehane *et al*. (2014). The lateral bearing capacity in the dimensionless form of the hybrid foundation is 60.78 at the tower rotation limit of 5° calculated by Eq. (2). The corresponding load bearing capacity is 63.34 from the centrifuge test data. In general, the empirical formulae result shows very good agreement with the centrifuge test data of the monopile-friction wheel hybrid foundation, providing confidence to the use the formulae for design guidance of this innovative hybrid foundation.

Table 1 Summary of FE analyses performed on lateral capacity of hybrid foundation

Analysis	D_w/L	L/D_p	φ	h/D_p	T_s/L	V (MN)	T_w/D_p	kD_p/s_{um}	Notes
Group I	0.52	13	31°	8.5	0.5	0	0.42	0.015	Comparison with model test data in this study
Group II	0.67	9	31°	15	0.5	5	0.63	0.13	Failure mechanism of hybrid foundation in sand overlaying clay
Group III	0.67	9	31°	15	1	5	0.63	0	Failure mechanism of hybrid foundation in sand
Group IV	0.67	9	31°	15	0	5	0.63	0.13	Failure mechanism of hybrid foundation in clay
Group V	0~0.72	7.5, 9, 10	31°	15	0.5	5	0.63	0.13	Investigation for the effect of wheel diameter
Group VI	0.67	7.5~10.5	31°	15	0.1, 0.5, 0.9	5	0.63	0.13	Investigation for the effect of pile length
Group VII	0.67	9	23°~40°	15	0.5	5	0.63	0.13	Investigation for the effect of φ
Group VIII	0.67	9	31°	11.3~30	0.5	5	0.63	0.13	Investigation for the effect of height of loading point
Group IX	0.67	9	31°	15	0~1	5	0.63	0.13	Investigation for the effect of thickness of sandy soil layer
Group X	0.67	9	31°	15	0.5	2~10	0.63	0.13	Investigation for the effect of pre-vertical load
Group XI	0.67	9	31°	15	0.5	5	0.25~1.63	0.13	Investigation for the effect of wheel thickness
Group XII	0.67	9	31°	15	0.5	5	0.63	0.18~0.2	Investigation for the effect of undrained shear strength of clay

Table 2 Values of coefficients to determine the lateral capacity of hybrid foundation in different conditions

			a	
T_s/L	$7.5 < L/D_p \le 8.5$	$8.5 < L/D_p \le 9.5$	$9.5 < L/D_p \le 10.5$	$10.5 < L/D_p \le 11.5$
(0.1, 0.3]	$a=-1.09-6.9\times\left(\frac{T_s}{L}\right)$	$a=3.89-40.35\times\left(\frac{T_s}{L}\right)$	$a=-2.01-190.55\times\left(\frac{T_s}{L}\right)$	$a=17.2-51.25\times\left(\frac{T_s}{L}\right)$
(0.3, 0.7]	$a=4.49-29.98\times\left(\frac{T_s}{L}\right)$	$a=-6.95-3.68\times\left(\frac{T_s}{L}\right)$	$a=-46.22-15.43\times\left(\frac{T_s}{L}\right)$	$a=7.52-19.5\times\left(\frac{T_s}{L}\right)$
(0.7, 1]	$a=-12.4-3.91\times\left(\frac{T_s}{L}\right)$	$a=-18.05+11.86\times\left(\frac{T_s}{L}\right)$	$a=21.27-107.24\times\left(\frac{T_s}{L}\right)$	$a=-33.95+39.75\times\left(\frac{T_s}{L}\right)$
			b	
T_s/L	$7.5 < L/D_p \le 8.5$	$8.5 < L/D_p \le 9.5$	$9.5 < L/D_p \le 10.5$	$10.5 < L/D_p \le 11.5$
(0.1, 0.3]	$b=36.67+129.4\times\left(\frac{T_s}{L}\right)$	$b=41.56+169.65\times\left(\frac{T_s}{L}\right)$	$b=124+170\times\left(\frac{T_s}{L}\right)$	$b=43+240\times\left(\frac{T_s}{L}\right)$
(0.3, 0.7]	$b=58.72+63.78\times\left(\frac{T_s}{L}\right)$	$b=80.17+40.63\times\left(\frac{T_s}{L}\right)$	$b=167.06+59.38\times\left(\frac{T_s}{L}\right)$	$b=99.75+52.5\times\left(\frac{T_s}{L}\right)$
(0.7, 1]	$b=65.87+50.34\times\left(\frac{T_s}{L}\right)$	$b=102.92+8.33\times\left(\frac{T_s}{L}\right)$	$b=48.71+225.71\times\left(\frac{T_s}{L}\right)$	$b=154.29-25.71\times\left(\frac{T_s}{L}\right)$
	$7.5 < L/D_p \le 8.5$	$8.5 < L/D_p \le 9.5$	$9.5 < L/D_p \le 10.5$	$10.5 < L/D_p \le 11.5$
c	0.81	0.87	1.04	1.23

7. Conclusions

This paper reports numerical modeling results about the behavior of monopile-friction wheel hybrid foundation under eccentric lateral load in sand-overlaying-clay conditions. An intensive parametric study is performed varying foundation geometry, sand properties, soil layer distribution, lateral loading height and pre-vertical load. The soil failure mechanism around the hybrid foundation is assessed, leading to an optimization foundation design. The following conclusions are obtained:

- Under the action of eccentric lateral load, failure of the hybrid foundation occurs under lateral and rotational movements. The plastic failure zone mainly develops

near the inner side of soil beneath the wheel edge in front of the loading direction, forming a shape similar to an inverted sector. "Punching-through" failure can be clearly captured with a thinner thickness of upper sandy layer.

- Increasing the wheel diameter leads to a pronounced increase of the load bearing capacity, especially beyond about half of pile embedment depth. The pile embedment depth (L/D_p) and internal friction angle of sand are positively correlated with the load bearing capacity of the foundation. The effect of soil layer distribution (T_s/L) can be divided into three main variation ranges. The ultimate lateral load capacity of the foundation reduces with the increase of loading height. The wheel thickness T_w has evident influence on the lateral capacity theoretically but should not be considered as the main design factors practically.
- Empirical formula is proposed to predict the load capacity of the hybrid foundation considering three different ranges of soil layer distribution for sand-overlaying-clay.

Acknowledgments

The first three authors of this paper were financially supported by the National Natural Science Foundation of China (Grant No. 52178329, 51578231 & 42176224), Guangdong Basic and Applied Basic Research Foundation (2021A1515010828) and Guangdong Provincial Key Laboratory of Modern Civil Engineering Technology (2021B1212040003).

References

Anastasopoulos, I. and Theofilou, M. (2016), "Hybrid foundation for offshore wind turbines: Environmental and seismic loading", *Soil. Dyn. Earthq. Eng.*, **80**, 192-209. https://doi.org/10.1016/j.soildyn.2015.10.015.

API (American Petroleum Institute). (2014). *ANSI/API recommended practice*, 2GEO, 1st Ed., Part 4, 499 Washington, DC.

Arshi, S. (2016), "Physical and Numerical Modelling of Hybrid Monopiled-Footing Foundation Systems", Ph.D. Dissertation; University of Brighton, Brighton, England.

Bandyopadhyay, S., Sengupta, A. and Parulekar, Y.M. (2020), "Behavior of a combined piled raft foundation in a multi-layered soil subjected to vertical loading", *Geomech. Eng.*, **21**(4), 379-390. https://doi.org/10.12989/gae.2020.21.4.379.

Chen, D., Gao, P., Huang, S.S., Li, C.S. and Yu, X.G. (2020), "Static and dynamic loading behavior of a hybrid foundation for offshore wind turbines", *Mar. Struct.*, **71**, 102727. https://doi.org/10.1016/j.marstruc.2020.102727.

Chong, S.H., Shin, H.S. and Cho, G.C. (2019), "Numerical analysis of offshore monopile during repetitive lateral loading", *Geomech. Eng.*, **19**(1), 79-91. https://doi.org/10.12989/gae.2019.19.1.079.

Dassault Systèmes. Abaqus analysis user's manual. Simulia Corp 2016.

DNV (Det Norske Veritas). (2019). *Offshore soil mechanics and geotechnical engineering*, DNV GL-RP-C212. Høvik, Norway: DNV.

El-Marassi, M. (2011), "Investigation of Hybrid Monopile-footing Foundation Systems Subjected to Combined Loading", Ph.D. Dissertation, The University of Western Ontario, Ontario, Canada.

Fatahi, B., Basack, S., Ryan, P., Zhou, W.H. and Khabbaz, H. (2014), "Performance of laterally loaded piles considering soil and interface parameters", *Geomech. Eng.*, **7**(5), 495-524. https://doi.org/10.12989/gae.2014.7.5.495.

Feng, X., Randolph, M.F., Gourvenec, S. and Wallerand, R. (2014), "Design approach for rectangular mudmats under fully three-dimensional loading", *Géotechnique*, **64**(1), 51-63. https://doi.org/10.1680/geot.13.P.051.

Gourvenec, S.M and Barnett, S. (2011). "Undrained failure envelope for skirted foundations under general loading", *Géotechnique*, **61**(3), 263-270. https://doi.org/10.1680/geot.9.T.027.

Gourvenec, S.M. and Mana, D. (2011), "Undrained vertical bearing capacity factors for shallow foundations", *Géotechnique Lett.*, **1**(4), 101-108. https://doi.org/10.1680/geolett.11.00026.

Hossain, M.S., Hu, P., Cassidy, M.J., Menzies, D. and Wingate, A. (2019), "Measured and calculated spudcan penetration profiles for case histories in sand-over-clay", *Appl. Ocean Res.*, **82**, 447-457. https://doi.org/10.1016/j.apor.2018.10.027.

Lehane, B.M., Pedram, B., Doherty, J.A. and Powrie, W. (2014), "Improved performance of monopiles when combined with footings for tower foundations in sand", *J. Geotech. Geoenviron. Eng.*, **140**(7), 04014027. https://doi.org/10.1061/(ASCE)GT.1943-5606.0001109.

Liu, F., Yi, JT., Cheng, P. and Yao, K. (2020), "Numerical simulation of set-up around shaft of XCC pile in clay", *Geomech. Eng.*, **21**(5), 489-501. https://doi.org/10.12989/gae.2020.21.5.489.

Li, D.Y., Feng, L.Y. and Zhang, Y.K. (2014), "Model tests of modified suction caissons in marine sand under monotonic lateral combined loading", *Appl. Ocean Res.*, **48**, 137-147. https://doi.org/10.1016/j.apor.2014.08.005.

Li, X.Y, Zeng, X.W. and Wang X.F. (2020), "Feasibility study of monopile-friction wheel-bucket hybrid foundation for offshore wind turbine", *Ocean Eng.*, **204**, 107276. https://doi.org/10.1016/j.oceaneng.2020.107276.

Li, X., Hu, Y. and White, D. (2013), "A large deformation finite element analysis solution for modelling dense sand", In *Proceedings of the 18th International Conference on Soil Mechanics and Geotechnical Engineering: Challenges and Innovations in Geotechnics,* Presses des Ponts. (1), 2359-2362. http://eprints.soton.ac.uk/id/eprint/419746.

Malhotra, S. (2011), Selection, design and construction of offshore wind turbine foundations. In *Wind turbines*, ed. I. Al-Bahadly. Rijeka, Croatia: InTech.

Meyerhof, G.G. and Hanna, A.M (1978), "Ultimate bearing capacity of foundations on layered soils under inclined load", *Can. Geotech. J.*, **15**(4), 565-572. https://doi.org/10.1139/t78-060.

Pedram, B. (2018), "Behaviour of Hybrid Piled Footing Structures in Sands", *Geotech Geol. Eng.*, **36**(4), 2273-2292. https://doi.org/10.1007/s10706-018-0461-7.

Raj, D., Singh, Y. and Kaynia, A.M. (2019), "Behavior and critical failure modes of strip foundations on slopes under seismic and structural loading", *Int. J. Geomech.*, **19**(6), 04019047. https://doi.org/10.1061/(ASCE)GM.1943-5622.0001427.

Stone, K.J., Arshi, H.S. and Zdravkovi, L. (2018), "Use of a bearing plate to enhance the lateral capacity of monopiles in sand", *J. Geotech. Geoenviron. Eng.*, **144**(8), 04018051. https://doi.org/10.1061/(ASCE)GT.1943-5606.0001913.

Trojnar, K. (2019), "Multi scale studies of the new hybrid foundations for offshore wind turbines", *Ocean Eng.*, **192**,

106506. https://doi.org/10.1016/j.oceaneng.2019.106506.
Wang, L.Z., Wang, H., Zhu, B. and Hong, Y. (2018b), "Comparison of monotonic and cyclic lateral response between monopod and tripod bucket foundations in medium dense sand", *Ocean Eng*., **155**, 88-105. https://doi.org/10.1016/j.oceaneng.2017.12.006.
Wang, X.F., Zeng, X.W., Yang, X. and Li, J.L. (2018a), "Feasibility study of offshore wind turbines with hybrid monopile foundation based on centrifuge modeling", *Appl. Energy*, **209**(1), 127-139. https://doi.org/10.1016/j.apenergy.2017.10.107.
Xu, C.J., Ding, H.B., Luo, W.J.,Tong, L., Chen, Q.S. and Deng, J.L.(2020) "Experimental and numerical study on performance of long-short combined retaining piles", *Geomech. Eng*., **20**(3), 255-265. https://doi.org/10.12989/gae.2020.20.3.255.
Yang, X., Wang, X.F. and Zeng X.W. (2017), "Numerical Simulation of the Lateral Loading Capacity of a Bucket Foundation", *Geotechnical Special Publication*, **279**, 112-121.
Yang, X., Zeng, X.W., Wang, X.F. and Yu, H. (2018), "Performance of monopile-friction wheel foundations under lateral loading for offshore wind turbines", *Appl. Ocean Res*., **78**, 14-24. https://doi.org/10.1016/j.apor.2018.06.005.
Zhou, M., Hossain, M.S., Hu, Y.X. and Liu, H. (2016), "Scale issues and interpretation of ball penetration in stratified deposits in centrifuge testing", *J. Geotech. Geoenviron. Eng*., **142**(5) 04015103. https://doi.org/10.1061/(ASCE)GT.1943-5606.0001442.
Zheng, G., Zhao, J.P., Zhou, H.Z. and Zhang, T.Q. (2018), "Ultimate Bearing Capacity of Strip Footings on Sand Overlying Clay Under Inclined Loading", *Comput. Geotech*., **106**, 266-273. https://doi.org/10.1016/j.compgeo.2018.11.003.
Zou, X.J., Hu, Y.X., Hossain, M. and Zhou, M. (2018), "Capacity of skirted foundations in sand-over-clay under combined V-H-M loading", *Ocean Eng*., **159**(1), 201-218. https://doi.org/10.1016/j.oceaneng.2018.04.007.

CC